Nanoscale

RSC Publishing

PAPER

Formation of single layer graphene on nickel under far-from-equilibrium high flux conditions†

Cite this: *Nanoscale*, 2013, **5**, 7250

Erik C. Neyts,*[a] Adri C. T. van Duin[b] and Annemie Bogaerts[a]

Received 9th January 2013
Accepted 25th April 2013

DOI: 10.1039/c3nr00153a

www.rsc.org/nanoscale

We investigate the theoretical possibility of single layer graphene formation on a nickel surface at different substrate temperatures under far-from-equilibrium high precursor flux conditions, employing state-of-the-art hybrid reactive molecular dynamics/uniform acceptance force bias Monte Carlo simulations. It is predicted that under these conditions, the formation of a single layer graphene-like film may proceed through a combined deposition–segregation mechanism on a nickel substrate, rather than by pure surface segregation as is typically observed for metals with high carbon solubility. At 900 K and above, nearly continuous graphene layers are obtained. These simulations suggest that single layer graphene deposition is theoretically possible on Ni under high flux conditions.

The segregation of graphene and graphite at metallic surfaces and grain boundaries at elevated temperatures has been known for decades.[1] The isolation of graphene at room temperature, however, has opened up an entirely new field in solid state physics,[2,3] thanks to its unique properties including quantum electronic transport, tunable band gap, extremely high mobility or electromechanical modulation.[4–7] As a result, various preparation techniques have been developed, including mechanical exfoliation, ultra high vacuum annealing of SiC, surface segregation followed by precipitation from metallic surfaces, and chemical reduction of graphene oxide.[3,8–10]

The metal-catalyzed growth of graphene has been demonstrated by several groups.[3,11,12] Major advantages of such processes are that they can proceed at ambient pressure and the metallic films are widely available. This allows an inexpensive and high-throughput growth of graphene. Furthermore, they allow the growth of patterned samples[13] beneficial for device fabrication.

The growth mechanism of graphene on Ni films was experimentally determined to be surface segregation rather than a deposition process, both at ambient pressure and at low pressure.[11,12] After the decomposition of the hydrocarbon source gas at the metallic surface, the carbon dissolves and diffuses through the subsurface and bulk regions, subsequently leading to graphene formation through a C segregation and precipitation process. It was found that the cooling rate is crucial for controlling the number of graphene layers.

On the simulation aspects, graphene formation and healing of defects on Ni(111) surfaces was previously simulated by Amara *et al.* using a grand canonical Monte Carlo tight binding model.[14,15] Amara *et al.* also studied the interaction between graphitic patches and a Ni(100) surface.[16] Gao *et al.* simulated the formation of small carbon clusters on a Ni(111) surface by density functional theory (DFT), emphasizing the role of pentagons and metal step edges in the graphene island formation.[17,18] The important role of Ni in catalytically healing defects in the carbon network at its surface was recently highlighted in simulations on the growth of single walled carbon nanotubes on small Ni clusters.[19–21]

However, studies focussing on the thermodynamic stability of preformed structures cannot provide information on the dynamics of the growth process itself. Monte Carlo studies can also not address the dynamics inherent to the growth process. For this purpose, molecular dynamics (MD) simulations can be applied. Meng *et al.*[22] used MD simulations based on the same Reax force field as used in the current work to study the graphene formation on Ni(111) at different temperatures, from a collection of pre-adsorbed C-atoms corresponding to different concentrations. High C-concentrations were found to be a requirement for graphene formation, and an optimal growth temperature of 1000 K was identified. To the best of our knowledge, however, studies focussing on the actual graphene growth process (*i.e.*, from sequential C-additions in which the C-concentration changes naturally) using MD simulations have not yet been carried out.

It should be mentioned that MD growth simulations invariably correspond to unrealistically high precursor fluxes to the substrate, leading to highly defective structures. Indeed, typical fluxes in the MD simulations are around 1 molecule per square nm and per ps, which corresponds to a pressure of at least one or two orders of magnitude higher than in typical

[a]*Department of Chemistry, University of Antwerp, Research group PLASMANT, Universiteitsplein 1, 2610 Antwerp, Belgium. E-mail: erik.neyts@ua.ac.be*

[b]*Department of Mechanical and Nuclear Engineering, The Pennsylvania State University, 136 Research Building East, University Park, Pennsylvania 16801, USA*

† Electronic supplementary information (ESI) available. See DOI: 10.1039/c3nr00153a

experiments. To overcome this problem, we here use hybrid molecular dynamics/uniform acceptance force bias Monte Carlo (MD/UFMC) simulations[20–23] for the formation of graphene on ultra-thin Ni(100) films.

As the UFMC implementation used in this work does not have an associated time scale,[24,25] the precise value of the impingement flux is undefined. It is, however, in any case much lower than in pure MD simulations, but most probably still higher than typical experimental fluxes. Thus, while structural relaxation is taken into account by virtue of the MC module, these simulations still correspond to relatively high precursor flux conditions. This simulation setup therefore experimentally corresponds to a single high-density, short pulse (nano- or microsecond) of growth precursor to the substrate.

In this work, we have deliberately chosen to simulate the growth on the Ni(100) facet, instead of the more stable Ni(111) facet, since it is known that on poly-Ni substrates, the most abundant (110) direction, in addition to the (100) and (111) directions, is transformed into the most abundant (100) direction after graphene synthesis.[26] Note that the Ni(100) surface is less closely packed compared to the Ni(111) structure. Therefore, the carbon diffusion barriers for segregation will be smaller on the Ni(100) surface.

Experimentally, it is known that in the segregation process of graphene on nickel surfaces, typically multiple graphene layers are formed.[3,27] This is a direct consequence of the relatively high solubility of carbon in bulk nickel, of about 2.7 at% at the eutectic point (1600 K) and 0.9 at% at about 900 K. In the subsurface region, the solubility is even much higher, reaching up to 25%, corresponding to the metastable Ni_3C composition.[20,28] Limiting the amount of carbon that can dissolve in the nickel might therefore avoid the formation of multiple layers and therefore result in single-layer graphene growth. The most straightforward way to accomplish this would be to reduce the thickness of the nickel film. However, while physical vapor deposited nickel films as thin as 1 nm have previously been used for CNT synthesis[29,30] such thin films inevitably form clusters when heated. Alternatively, the dissolution of carbon in the film may also be limited by very rapidly saturating the upper layers of the film, before diffusion to the bulk takes place. In this scenario, advantage is taken of the relatively high barrier for diffusion of surface adsorbed carbon into the bulk of the nickel substrate and for diffusion from the bulk to the surface, which has an overall value of about 2.33 eV.[31] In this paper, we demonstrate that such a rapid saturation indeed leads to another graphene growth mechanism, *i.e.*, based on combined deposition–segregation, instead of the typical segregation process under standard CVD conditions. This corresponds to a growth system under far from equilibrium conditions, as can be approximated by the high precursor flux in the MD simulations. We demonstrate here that this combined deposition–segregation mechanism can indeed result in the formation of single-layer graphene.

The methodology applied to simulate the graphene growth is similar to the one used previously for the simulation of single-walled carbon nanotube growth.[20,21,23] In short, our simulations are based on the Reax Force Field (ReaxFF) potential,[32] employing recently developed force field parameters for Ni/C.[33] In the hybrid MD/UFMC simulation, MD and UFMC stages are alternating, each providing the input structure for the next stage.[20,24,34] Each MD stage runs for 4 ps using a timestep of 0.25 fs employing a velocity Verlet integration scheme. Temperature and pressure are controlled using the Berendsen thermostat and barostat with coupling constants of 100 fs and 1000 fs, respectively. The temperatures investigated are varied between 300 K and 1500 K. Employing the barostat allows us to generate zero stress structures at all temperatures. The substrate is a Ni(100) structure with a thickness of about 6 Å, corresponding to 4 atomic layers of 50 atoms each, covering a total surface area of about 317 $Å^2$. As this substrate is much thinner than a typical experimental thickness, the lowest atomic layer was kept fixed in order to mimic a (infinitely) thick substrate. This lower atomic layer also serves as an impenetrable barrier for bulk diffusion, as a first approximation to take into account the much lower C solubility in the bulk of the Ni crystal compared to the subsurface area, while still correctly accounting for the subsurface area itself. Periodic boundaries are applied in the lateral directions to simulate a semi-infinite surface.

Growth is accomplished by adding new gas phase carbon atoms to the simulation box every 2 ps at a minimum distance of 5 Å above the surface of the film and with random $\{x,y\}$ coordinates. In total, 3195, 2733, 2428, 2268, 1857, 1679 and 1895 carbon atoms were added to the simulation box during the runs at 300 K, 500 K, 700 K, 900 K, 1100 K, 1300 K, and 1500 K, respectively, resulting in the incorporation of 107, 157, 172, 196, 199, 223 and 180 carbon atoms, respectively.

In Fig. 1, the evolution of the graphene growth process on a Ni(100) surface as emerging from the simulations is illustrated for a growth temperature of 900 K. A similar evolution is observed at the other temperatures investigated, except at 300 K where no graphene sheet or even graphitic-like patches are formed (see below). The observed growth process is as follows. Initially (Fig. 1a), the impinging carbon atoms adsorb on the surface, where they diffuse either from surface site to surface site, as well as to subsurface sites. As the concentration of carbon at the surface increases (due to the continued addition of carbon atoms from the gas phase), also the occupation of the subsurface sites rises, along with the appearance of the first dimers and trimers at the surface (see Fig. 1a). These surface dimers and trimers are observed to be highly mobile, particularly at higher temperatures (*i.e.*, 900 K and above). In agreement with the results obtained by Meng *et al.* on the Ni(111) surface,[22] this results in a disordered surface structure, with most of the C-atoms being sp-hybridized. Subsequently, longer and branched chains up to 5 or 6 carbon atoms start to appear (see Fig. 1b). These chains virtually always adopt valence angles of about 120°. Some of these chains fold with the formation of the first rings (see Fig. 1b), which serve as the initial nuclei from which a graphene sheet can grow in a later stage. A further increase in the number of carbon atoms allows these first rings and surface chains to grow until they meet (see Fig. 1c and d). This growth process finally leads to the formation of an almost complete graphene-like layer, on top of a carbon saturated Ni-crystal surface (see Fig. 1f). A similar behaviour, resulting in the

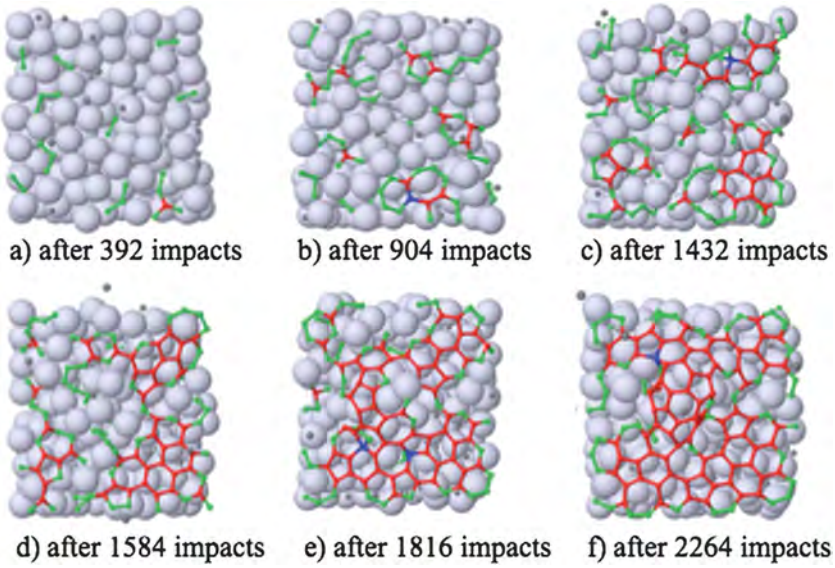

Fig. 1 Evolution of the graphene growth process on a Ni(100) surface in top view at 900 K. The large grey spheres represent Ni atoms. The small grey, green, red and blue spheres represent free, 1- and 2-coordinated, 3-coordinated, and 4-coordinated C atoms, respectively. Note that green C atoms near the edges are in fact 3-coordinated through the lateral periodic boundaries.

formation of a graphene-like overlayer, is predicted by our simulations at all temperatures above 700 K (see below).

A graphical representation, both in side view and top view, of the final states of the MD/UFMC simulations is presented in Fig. 2 for all temperatures investigated in this work in the range $T = 300$–1500 K.

At the lowest investigated temperature (300 K), the resulting carbon network structure is very defective. At this temperature, the first dimers and trimers are formed by the impingement of carbon atoms in the vicinity of already incorporated carbon atoms. Due to the very limited solubility of carbon in nickel at low temperature ($\ll$1% at room temperature for bulk Ni), and due to the very limited mobility of the carbon atoms at low temperature (*i.e.*, the diffusion coefficient of C in Ni is about 8.5×10^{-30} m^2 s^{-1} at 300 K) the surface and subsurface area quickly become saturated and the formation of a carbon network at the surface is essentially determined by the consecutive and intrinsically random impingement locations of the carbon atoms from the gas phase. As a result, the network formed at this temperature consists of long branched polyyne chains, and a few rings, but no graphene. Furthermore, the low temperature inhibits the metal-mediated healing of defects, which was observed to be operative at higher temperatures.[20,21]

Increasing the temperature to 500 K and 700 K, however, leads to a different scenario. Indeed, starting from 500 K, the carbon atoms seem to be sufficiently mobile to wander over the surface and attach to growing ring structures. Now the first dimers and trimers are not only formed by the impingement of carbon atoms close to other carbon atoms, but also because of the increased mobility of the carbon atoms. Due to the high carbon flux towards the substrate, saturation is quickly reached. As mentioned above, the fixed layer of Ni-atoms serves as an impenetrable barrier for bulk diffusion. This approach should be regarded as a first approximation only to the limited bulk solubility (particularly in view of the much higher solubility of the subsurface layers), as it effectively reduced the number of carbon atoms needed to impinge on the surface before saturation occurs. Newly added carbon atoms are therefore deposited on the surface, instead of diffusing to the subsurface, as will be further demonstrated below. The higher temperature of 500 K and above also aids in the metal-mediated healing of defects, as we have also observed earlier in the growth of single-walled carbon nanotubes on Ni-clusters,[20,21] and as was also observed by Page *et al.* in DFTB simulations.[19] However, up to a temperature of 700 K, we do not observe the formation of a continuous graphene or defected graphene-like layer.

At a growth temperature in the range of 900–1500 K, we observe the formation of nearly continuous graphene layers, as illustrated in Fig. 1. The mechanism appears to be the same in this entire temperature range. At these temperatures, the carbon atoms are sufficiently mobile at the surface and in the first subsurface layer, so they can easily find energetically stable positions, thereby forming graphene more easily than at lower temperatures. Moreover, higher temperatures also enhance the metal mediated defect healing, as this is related to the diffusivity of the metal atoms. The optimal temperature in our simulations was found to be around 1100 K. This can be compared with the temperature of 1000 K found by Meng *et al.* as the optimal growth temperature on Ni(111).[22] No simulations were carried out above 1500 K, because at higher temperatures the surface layer starts to melt (the melting temperature of bulk nickel is 1726 K).

It is worth mentioning that at 900 K, an additional process was observed in our simulations. As can be seen in Fig. 2, a single walled carbon nanotube (SWNT) cap nucleates during the graphene growth process. Usually, SWNTs nucleate when carbon atoms form a hexagonal network on a curved metal particle, which subsequently lifts off from the surface of the

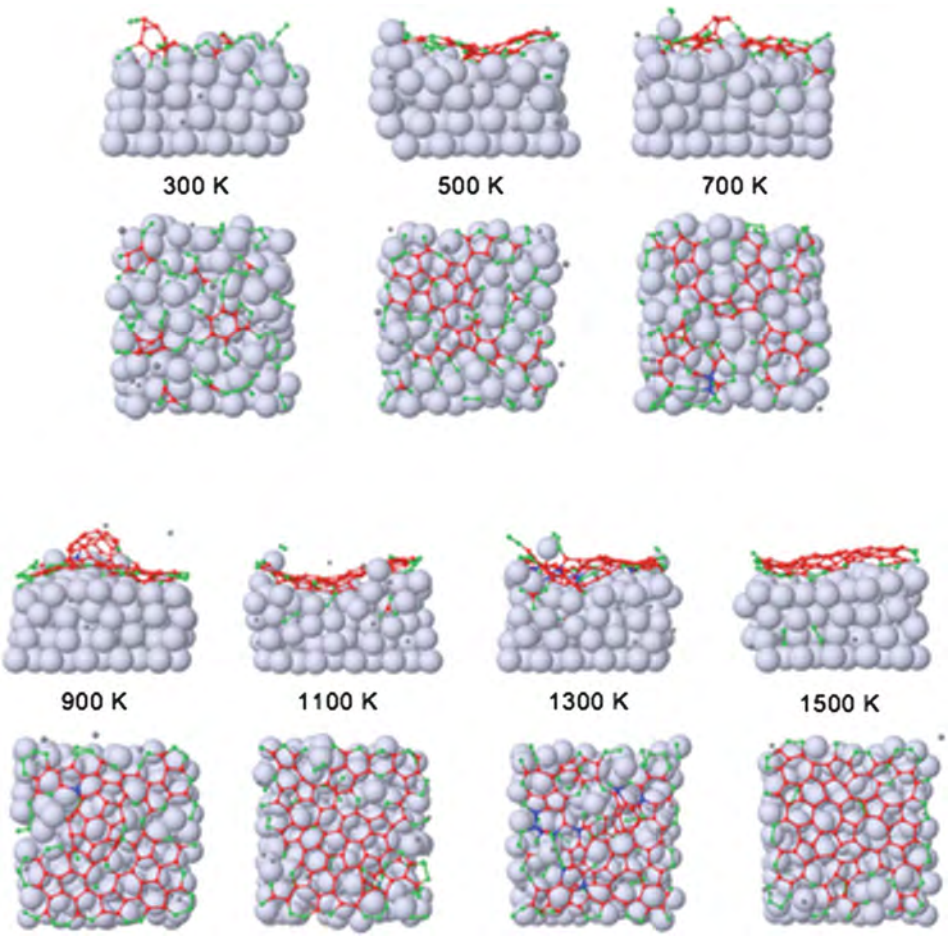

Fig. 2 Final configurations of the graphene layers (or carbon layers) grown on a Ni(100) surface, for the various substrate temperatures investigated, both in side view and top view. The color-coding is the same as in Fig. 1.

particle. In this particular simulation, two more or less flat graphene patches are first formed, which grow towards each other. The surface structure is destabilized and becomes disordered due to the dissolution of the carbon. Indeed, previously we have demonstrated that dissolving C in pure Ni leads to an effective liquefaction of the cluster.[35] Thermal fluctuations in this highly mobile and disordered surface structure lead to the formation of small bumps on the surface. As the patches grow and merge, they form a layer partially covering the little bump, such that a small SWNT cap is formed, while new carbon atoms can still be added. This concurrent CNT and graphene formation has also been observed experimentally.[36]

The time-evolution of the carbon network growth at 900 K and 1500 K is depicted in Fig. 3. For the sake of clarity, the Ni atoms are not shown here. The C atoms are white-to-red color-coded according to the time of their addition to the system.

Initially, all impinging carbon atoms dissolve into the first subsurface layer, and subsequently also in the second subsurface layer (colored white). When these layers become saturated, the additionally added carbon is mostly deposited on the surface, as evidenced by the absence of red atoms in the bulk. Indeed, under the high flux conditions adopted in this work (see above), the carbon atoms cannot quickly enough overcome the energy barrier for diffusion to the bulk of 2.33 eV,[31] and thus they remain immobile in the time frame of the simulation and in the time frame needed for the first carbon surface layer to form. This can be seen in the figure, as almost all carbon atoms colored red are found in the graphene layer, corresponding to the atoms added later in the simulation, after the initial saturation of the subsurface layers. However, the graphene layer also contains a significant number of white colored atoms, *i.e.*, atoms that segregated from the bulk. This suggests that the

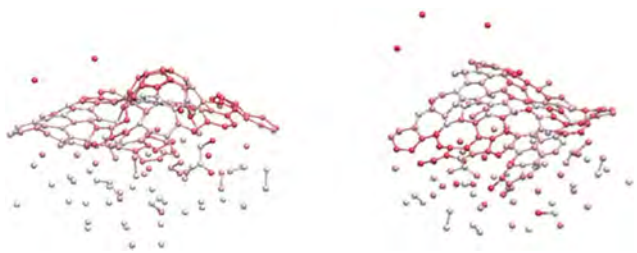

Fig. 3 Visualization of the time-evolution of the obtained carbon network at 900 K (left) and 1500 K (right), colored according to the time of C addition to the system. The white atoms were added first; the red atoms were added last. The Ni atoms are not shown here, for the sake of clarity.

growth mechanism of the graphene network is a combined deposition–segregation mechanism. To the best of our knowledge, experiments employing a single pulse of growth precursor at high density, as simulated in this work, have not yet been carried out, and consequently this phenomenon has not yet been observed. This phenomenon is indeed directly related to the far-from-equilibrium, high flux conditions adopted in our simulations (see ESI†). In contrast, under low flux conditions, which are commonly used in experiments up to now, the nickel film can serve as a sink, in which additional carbon atoms can dissolve, and from which previously added carbon atoms can segregate. However, our simulations point out that if experimentally the nickel film can be quickly saturated, a combined deposition–segregation mechanism could occur, and single-layer graphene could be formed.

The ratio of "deposited" atoms to "segregated" atoms in our simulations decreases with increasing temperature, from 0.49 at 300 K over 0.41 at 900 K to 0.36 at 1500 K. Indeed, at lower temperature, the carbon solubility is much lower than at higher temperature, so that the deposition occurs relatively faster at lower temperature. In other words, graphene formation by a segregation mechanism is favoured at high temperature and low impinging particle flux (as is known experimentally), while a combined segregation–deposition mechanism is favoured at lower temperatures (around 700–900 K) and high impinging particle flux (following the mechanism discussed above). Finally note that the temperature cannot be set too low, as this would prevent surface diffusion as well as metal-mediated defect healing.

In summary, hybrid reactive MD/MC simulations are performed to investigate the growth of single layer graphene on a Ni(100) film in the temperature range 300–1500 K under far-from-equilibrium high precursor flux conditions. At the lowest temperature (300 K), no graphene network was obtained. At 500 K and 700 K, graphitic islands are formed, while at 900 K and above, the formation of nearly continuous graphene layers is observed. Our simulations suggest that, under these conditions, the graphene network is formed by a combination of depositing carbon atoms and carbon atoms segregating at the surface from subsurface sites. It is found that the ratio of deposited carbon atoms to segregated carbon atoms decreases upon increasing temperature. These results open prospects to control the graphene growth mechanism by control over the substrate temperature and impinging particle fluxes.

Acknowledgements

This work was carried out in part using the Turing HPC infrastructure at the CalcUA core facility of the Universiteit Antwerpen, a division of the Flemish Supercomputer Center VSC, funded by the Hercules Foundation, the Flemish Government (department EWI) and the Universiteit Antwerpen.

References

1 J. C. Shelton, H. R. Patil and J. M. Blakely, *Surf. Sci.*, 1974, **43**, 493–520.
2 A. K. Geim and K. S. Novoselov, *Nat. Mater.*, 2007, **6**, 183–191.
3 K. S. Kim, Y. Zhao, H. Jang, S. Y. Lee, J. M. Kim, K. S. Kim, J.-H. Ahn, P. Kim, J.-Y. Choi and B. H. Hong, *Nature*, 2009, **457**, 706–710.
4 Y. Zhang, Y. W. Tan, H. L. Stormer and P. Kim, *Nature*, 2005, **438**, 201–204.
5 M. Y. Han, B. Oezyilmaz, Y. Zhang and P. Kim, *Phys. Rev. Lett.*, 2007, **98**, 206805.
6 K. I. Bolotin, K. J. Sikes, Z. Jiang, M. Klima, G. Fudenberg, J. Hone, P. Kim and H. L. Stormer, *Solid State Commun.*, 2008, **146**, 351–355.
7 J. S. Bunch, A. M. van der Zande, S. S. Verbridge, I. W. Frank, D. M. Tanenbaum, J. M. Parpia, H. G. Craighead and P. L. McEuen, *Science*, 2008, **315**, 490–493.
8 X. Li, G. Y. Zhang, X. D. Bai, X. M. Sun, X. R. Wang, E. Wang and H. J. Dai, *Nat. Nanotechnol.*, 2008, **3**, 538–542.
9 G. Eda, G. Fanchini and M. Chhowalla, *Nat. Nanotechnol.*, 2008, **3**, 270–274.
10 M. Xu, D. Fujita, K. Sagisaka, E. Watanabe and N. Hanagata, *ACS Nano*, 2011, **5**, 1522–1528.
11 X. Li, W. Cai, L. Colombo and R. S. Ruoff, *Nano Lett.*, 2009, **9**, 4268–4272.
12 Q. Yu, J. Lian, S. Siriponglert, H. Li, Y. P. Chen and S. S. Pei, *Appl. Phys. Lett.*, 2008, **93**, 113103.
13 A. Reina, X. Jia, J. Ho, D. Nezich, H. Son, V. Bulovic, M. S. Dresselhaus and J. Kong, *Nano Lett.*, 2009, **9**, 30–35.
14 H. Amara, C. Bichara and F. Ducastelle, *Phys. Rev. B: Condens. Matter Mater. Phys.*, 2006, **73**, 113404.
15 H. Amara, J.-M. Roussel, C. Bichara, J.-P. Gaspard and F. Ducastelle, *Phys. Rev. B: Condens. Matter Mater. Phys.*, 2009, **79**, 014109.
16 H. Amara, C. Bichara and F. Ducastelle, *Surf. Sci.*, 2008, **602**, 77–83.
17 J. Gao, Q. Yuan, H. Hu, J. Zhao and F. Ding, *J. Phys. Chem. C*, 2011, **115**, 17695–17703.
18 J. Gao, J. Yip, J. Zhao, B. I. Yakobson and F. Ding, *J. Am. Chem. Soc.*, 2011, **133**, 5009–5013.
19 A. J. Page, Y. Ohta, Y. Okamoto, S. Irle and K. Morokuma, *J. Phys. Chem. C*, 2009, **113**, 20198–20207.
20 E. C. Neyts, Y. Shibuta, A. C. T. van Duin and A. Bogaerts, *ACS Nano*, 2010, **4**, 6665–6672.
21 E. C. Neyts, A. C. T. van Duin and A. Bogaerts, *J. Am. Chem. Soc.*, 2011, **133**, 17225–17231.
22 L. Meng, Q. Sun, J. Wang and F. Ding, *J. Phys. Chem. C*, 2011, **116**, 6097.
23 E. C. Neyts, A. C. T. van Duin and A. Bogaerts, *J. Am. Chem. Soc.*, 2012, **134**, 1256.
24 M. Timonova, J. Groenewegen and B. J. Thijsse, *Phys. Rev. B: Condens. Matter Mater. Phys.*, 2010, **81**, 144107.
25 E. C. Neyts, B. J. Thijsse, M. J. Mees, K. M. Bal and G. Pourtois, *J. Chem. Theory Comput.*, 2012, **8**, 1865–1869.
26 S. J. Chae, F. Günes, K. K. Kim, E. S. Kim, G. H. Han, S. M. Kim, H.-J. Shin, S.-M. Yoon, J.-Y. Choi, M. H. Park, *et al.*, *Adv. Mater.*, 2009, **21**, 2328–2333.
27 A. N. Obraztsov, E. A. Obraztsova, A. V. Tyurnina and A. A. Zolotukhin, *Carbon*, 2007, **45**, 2017–2021.

28 M. Diarra, A. Zappellli, H. Amara, F. Ducastelle and C. Bichara, *Phys. Rev. Lett.*, 2012, **109**, 185501.
29 C. Zhang, D. Cott, N. Chiodarelli, P. Vereecken, J. Robertson and C. M. Whelan, *Phys. Status Solidi B*, 2008, **245**, 2308–2310.
30 N. Chiodarelli, S. Masahito, Y. Kashiwagi, Y. Li, K. Arstila, O. Richard, D. J. Cott, M. Heyns, S. De Gendt, G. Groeseneken and P. M. Vereecken, *Nanotechnology*, 2011, **22**, 085302.
31 F. Abild-Pedersen, J. K. Norskov, J. R. Rostrup-Nielsen, J. Sehested and S. Helveg, *Phys. Rev. B: Condens. Matter Mater. Phys.*, 2006, **73**, 115419.
32 A. C. T. van Duin, S. Dasgupta, F. Lorant and W. A. Goddard III, *J. Phys. Chem. A*, 2001, **105**, 9396–9409.
33 J. E. Mueller, A. C. T. van Duin and W. A. Goddard III, *J. Phys. Chem. C*, 2010, **114**, 5675–5685.
34 M. J. Mees, G. Pourtois, E. C. Neyts, B. J. Thijsse and A. Stesmans, *Phys. Rev. B: Condens. Matter Mater. Phys.*, 2012, **85**, 134301.
35 E. Neyts, Y. Shibuta and A. Bogaerts, *Chem. Phys. Lett.*, 2010, **488**, 202–205.
36 A. Malesevic, R. Kemps, L. Zhang, R. Erni, G. Van Tendeloo, A. Vanhulsel and C. Van Haesendonck, *J. Optoelectron. Adv. Mater.*, 2008, **10**, 2052–2055.